Preprint typeset in JINST style - HYPER VERSION

CALICE Analysis Note CAN-061
v2
May 29, 2018

Timing of hadron showers in the CALICE Analog Hadronic Calorimeter prototype using steel absorber

The CALICE Collaboration*

This note contains preliminary CALICE results, and is for the use of members of the CALICE Collaboration and others to whom permission has been given.

ABSTRACT: This note presents results obtained with the CALICE Analog Hadronic Calorimeter prototype with steel absorber at the SPS CERN testbeam campaign in July 2015. The analysis presents the timing calibration and includes timing distributions for muon, electron and pion beams. The results are compared to several GEANT 4 version 10.1 physics lists.

*Corresponding authors: Eldwan Brianne (eldwan.brianne@desy.de), Katja Krüger (katja.krueger@desy.de)

Contents

1. Introduction **1**

2. Testbeam Setup **2**

3. Simulation **3**
3.1 Geometry and Digitization 3
3.2 AHCAL Model Validation 4

4. Event Selection **6**
4.1 Muon selection 6
4.2 Electron selection 6
4.3 Pion selection 6

5. Timing calibration of the AHCAL **7**
5.1 Time recording in the SPIROC2b 8
5.2 Timing calibration procedure 8
5.3 Slope and Pedestal extraction 9
5.4 Time reference calibration 9
5.5 Time offset correction 10
5.6 Non-linearity correction 11
5.7 Time-walk correction 12
5.8 Number of triggered channel in a chip correction 12

6. Results **15**
6.1 Systematic uncertainties 15
6.2 Timing of muon and electron beams 16
6.3 Timing of pion showers 17

7. Conclusion **21**

A. Appendix **23**

1. Introduction

Experiments at future lepton colliders require unprecedented jet energy resolution of 3-4% up to 250 GeV jet energies. The Particle Flow concept (PFAs) [1] aims to achieve such resolutions by combining measurements of the tracker and calorimeters. This requires exceptional granularity for the calorimeters. The CALICE Collaboration develops, builds and tests such calorimeters to fulfil

the requirements imposed by PFAs. One calorimeter concept is the Analog Hadronic Calorimeter (AHCAL) that consists of scintillator tiles of 3×3 cm^2 readout by Silicon Photomultipliers (SiPMs). Several prototypes with different absorbers, granularity and readout have been tested.

Apart from energy measurement, the aspect of precise timing measurement is being investigated. Timing measurements in a calorimeter can be used to reject out of time pile-up events. In addition, the impact of background events on physics measurements such as $\gamma\gamma \rightarrow$ hadrons background, could be mitigated by using timing information of the calorimeters and trackers [2]. Moreover, time information could be used to improve the energy reconstruction of hadronic showers by distinguishing the electromagnetic and hadronic components of the shower.[3].

The CALICE Analog Hadronic Calorimeter (AHCAL) prototype [4, 5] with steel absorber has been installed in the SPS CERN facilities in July 2015. This prototype was partially instrumented and was comprised of earlier version of active readout. The performance of this prototype is not expected to reach the final performance of the engineering prototype. Furthermore, this prototype was operated at a lower clock speed than the design in order to enhance the data taking efficiency which limits the timing resolution. This note presents the time calibration procedure of the AHCAL and the results obtained in muon, electron and pion beams in an energy range from 10 GeV to 90 GeV, as indicated in table 5 in the appendix. Furthermore, this analysis is the first of its kind to such a system level and enters new territories for high granular calorimeters.

2. Testbeam Setup

The testbeam setup at CERN in July 2015, at the SPS beamline H2, is shown in figure 1.

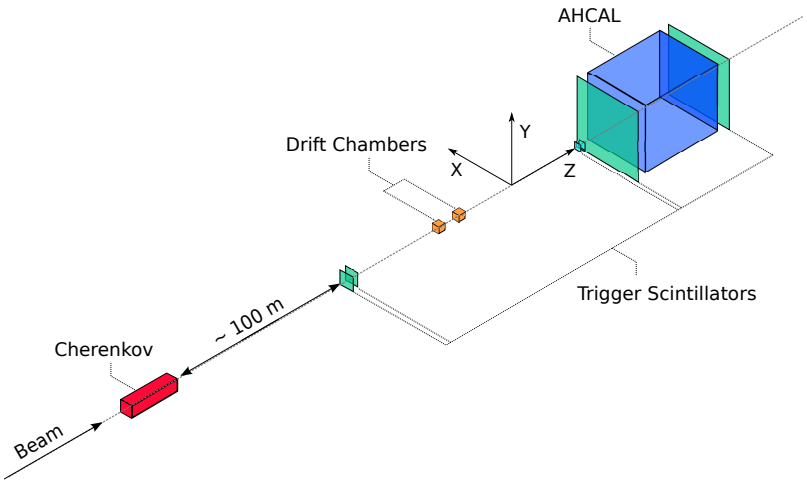

Figure 1: Sketch view of the beamline setup at the CERN SPS H2 beamline in July 2015.

The AHCAL prototype absorber stack is composed of 48 steel plates in which 14 active modules were installed. The two first modules consist of single ECAL Base Units (EBUs) with 4×36 cells of 4.5×0.5 cm^2 size (ECAL). The ECAL cells of both modules are oriented parallel to the x-axis. The next eight modules consist of single HCAL Base Units (HBUs) with 12×12 cells of 3×3 cm^2 size (HCAL). The absorber plates have thickness of 1.7 cm, such that the first 10 modules correspond to a depth of around 10 X_0 ($\sim 1\ \lambda_\pi$). These modules were mainly used as a shower start

finder. The last four modules consist of 2 by 2 HBUs providing information about the development of pion showers at different depths. In total, the prototype has 3744 channels. Table 1 provides an overview of the AHCAL layer structure. It uses SiPM technology coupled to scintillator tiles readout by an application specific integrated chip, the SPIROC2b [6]. A diverse variety of SiPMs and tile designs were used in this testbeam, a detailed table of the SiPM characteristics can be seen in Table 10. The AHCAL detector was placed on a movable stage in order to be able to scan the detector with muons for calibration runs.

Table 1: Layer structure of the AHCAL in July 2015.

Absorber Slot #	Layer #	Abs. thickness before layer [X_0/λ_π]	Layer size [cm^2]	N_{chn}
1-2	1-2	$\sim$1/0.1	18×18	288
3-10	3-10	$\sim$1/0.1	36×36	1152
11	11	$\sim$1/0.1	72×72	576
13	12	$\sim$2/0.2	72×72	576
21	13	$\sim$8/0.8	72×72	576
31	14	$\sim$10/1	72×72	576

Scintillator plates, $10 \times 10 cm^2$ and $50 \times 50 cm^2$, placed in front and back of the calorimeter are used as a trigger signal that is provided to the AHCAL DAQ to validate events [7]. Additionally, the coincidence signal from the scintillators is provided directly to several channels of the AHCAL in order to provide a reference time of the trigger as shown in table 6. A Cherenkov detector, at around 100 m upstream, was available to tag incoming particles.

3. Simulation

The AHCAL simulation model is based on the MOKKA [8] framework v08-05-01 and the new DD4HEP [9] framework v00-16, using the GEANT 4 v10.1 simulation [10]. A right-handed coordinate system is used such that the Z-axis points in the beam direction and that the Y-axis is directed upwards. No beamline instrumentation is simulated except scintillator triggers in front of and behind the detector. A similar amount of material is achieved by filling the world volume with air and by adding 5.6 mm of lead ($\sim 1\ X_0$) directly at the calorimeter front face in order to account for missing upstream material. The beam gun is placed 1 m from the calorimeter front face and it is configured to generate single beam particles with a 2% momentum spread according to the beamline parameters. Muons and electron showers are simulated using the QGSP_BERT_HP physics list. Pion showers are simulated using QGSP_BERT, QGSP_BERT_HP and QBBC physics lists.

The MOKKA and DD4HEP simulations have been checked to give consistent results. In the following, only the results with the DD4HEP simulation are shown if not specified.

3.1 Geometry and Digitization

The AHCAL simulation model consists of 32 absorber layers and 14 active modules. Each absorber layer are made of stainless steel 17.2 mm thick. Each active layer is primarily composed of 1 mm

steel cassette, 0.7 mm PCB, 2 or 3 mm scintillator strip or tile. The density and composition of the scintillator is taken as default provided in GEANT 4.

The digitization of simulated hits is very similar to the previous AHCAL physics prototype [11]. Individual calibration factors obtained from data are used to extract the light yield which is needed to model the statistical fluctuations of photons hitting a SiPM [12]. Saturation effects are also included using a global parameter, the number of pixels available on each SiPM type, as no measurement of the saturation curve is available. Most of the tiles used are wrapped with a reflective foil such that crosstalk effects between channels can be neglected. For modules with no wrapping, a default value of 15% for the cross-talk is used based on previous measurements with the AHCAL physics prototype [13]. A variation of the cross-talk parameter between 10% and 18% is used for systematics (see section 6.1). Noise is extracted from muon runs and overlaid onto simulated events. Dead channels and channels without calibration factors (MIP, gain, pedestal) are rejected.

The timing of simulated hits is modeled as in the SPIROC2b, the energy from sub-hits in a cell is integrated over a sliding time window of 15 ns, if the energy sum of the sub-hits in this time window passes the energy threshold, the time of the sub-hit passing the energy threshold is used as the time of the simulated hit. To simulate detector resolution effects, the time of a simulated hit is smeared with a double Gaussian function, with parameters determined from data, and is convoluted with a Gaussian function with a sigma depending on the number of triggered channels in a chip parametrized from data (see section 5.8).

After the digitization, all simulated hits have the same format as raw data hits and are reconstructed with the same software chain that is used for data. To suppress noise hits, only hits above 0.5 MIP are considered in this study.

3.2 AHCAL Model Validation

Prior to the time analysis, the simulation and digitization are validated. Comparisons of electromagnetic interactions in the AHCAL are done as such interactions should be well described in simulation. Firstly, the simulation must be validated at the lowest hit energies. The comparison of the spectrum of a MIP-like particle traversing the AHCAL was done and is shown in figure 2a. The shape of the spectrum matches relatively well. The simulation is slightly more narrow than the data because of channel-by-channel mis-calibrations that are not fully modeled in the simulation. The figure 2b shows the longitudinal mean energy profile for muon-like tracks in data and simulation. The data is reproduced by the simulations within 3-4%. Channels for which no calibration with MIP-like particles could be determined in data are excluded from the analysis in data and simulation. A systematic on the energy scale of the calorimeter as shown in table 4 is applied later on the data when looking at the dependence of the time as a function of the hit energy.

Further comparison were made using the electron dataset. Figure 3 shows the hit energy spectrum for 10 GeV electron showers in data and simulation. Hit energies up to 10 MIPs are well described by the simulation, with deviations up to 10%. In the region of 20 MIPs, where a larger difference is noticeable, the SPIROC2b switches from high gain to low gain readout. A mis-calibration of the factor between the two gains leads to the observed difference. At high hit energies above 60 MIPs, the simulation is underestimating the hit energy significantly. A similar effect is observed at higher beam energies. This effect is caused by a too small value of the number

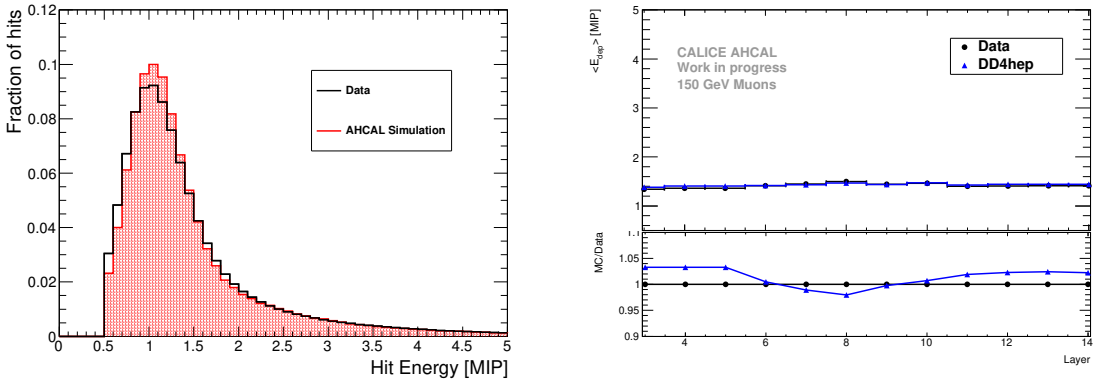

(a) (b)

Figure 2: a) Hit Energy Spectra for the complete AHCAL for muon like-track hits for both data and simulation. b) Longitudinal mean energy profile for muon like-track hits in data and the DD4HEP simulation.

of effective pixels used to simulate SiPM saturation effects. The nominal number of pixels is used, which does not take into account that pixels can fire more than once due to recovery and afterpulsing. However, for this analysis, only energies below tens of MIPs are relevant (see section 5.7) and well described by the simulation.

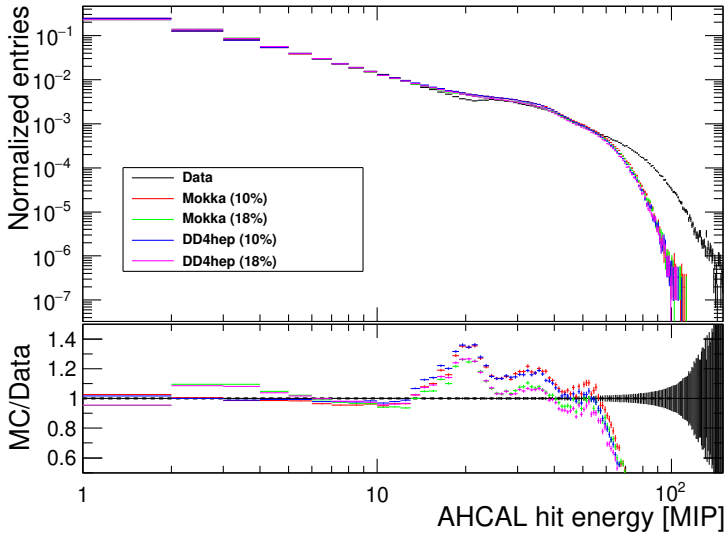

Figure 3: Electron hit energy spectra for data and simulation for 10 GeV beam energy. The different colors corresponds to the variation of the cross-talk parameter in the simulations between 10% and 18%.

For 10 GeV electrons, a 10% cross-talk value seems to be preferred by the data. However, for higher electron energies, a 18% cross-talk value seems to be favoured by the data. The data cannot be described in simulation by a global cross-talk parameter.

The simulation does not describe the data perfectly especially for higher electron beam energies. However, the description of electromagnetic showers in simulations is deemed satisfactory for the study of the time development of hadron showers.

4. Event Selection

4.1 Muon selection

To select muons, an event pre-selection and a track finder [12] selection is performed. A cut on the maximum number of hits in the AHCAL is done at 20 as the number of hits should be around 1 per layer for a MIP-like particle plus the number of noise hits expected in the detector. The track finder algorithm selects AHCAL towers of hits in the same $x : y$ position and it rejects AHCAL towers that contains less than a certain number of hits. In order to select muons or punch-through pions, a straight track of at least 7 hits is required in the whole AHCAL. This assumes that the calorimeter was perpendicular to the beam, any tilted tracks would be missed. In addition, to reject pion showering deep in the detector, no more than 2 hits are allowed per layer to account for some flexibility with noise hits. A summary of the muon selection is shown in table 7. The selection efficiency is 72.5% for muons, <0.1% for electrons and 5% for pions which is compatible with the fraction of pion traversing the AHCAL without hard interaction.

4.2 Electron selection

Electron events are needed to validate the timing behavior in simulation as well as the detector simulation model. It is important to have a clean sample of electrons to cross-check the timing calibration. An electron selection is done using the beam instrumentation and the AHCAL layer information. Events with a Cherenkov tag are used. The energy deposit in the first three AHCAL layers ($E_3 + E_4 + E_5$) must be over 10 MIPs. A box cut on the number of hits and the center of gravity in the z direction is done. As the number of hits in a electron shower increases with the shower energy, this cut is energy dependent. The energy deposited in the last two layers relative to the energy deposited in the calorimeter ($(E_{13} + E_{14})/\Sigma E$) is required to be under 1% to reject pion showers and to contain the electron shower. The electron selection is summarised in table 8. The selection efficiencies are shown in 2. Even though a significant fraction of pions passes the electron selection at low energies, there is confidence that very little pion contamination is present in the data due to the pure electron beam generation with the beamline.

4.3 Pion selection

The goal of the pion selection is to reject punch-through pions, muons and possible electron contamination as these events would be instantaneous. The events without a Cherenkov tag are selected. The number of hits per event needs to be above 20 to reject most muons or punch-through pions. No cut on the center of gravity in z is done in order not to bias the start of the pion shower. The energy fraction deposited in the two last AHCAL layers must be above 1% in order to ensure that the pion showered and to reject possible electron showers. The number of hits in the two first AHCAL layers $N_3 + N_4$ must be smaller than 5 to mitigate possible particle contamination from electrons. In addition, multiple particle events were observed in the data. As no beam instrumentation could be used for rejecting these events, a rejection method based on the hit time information

Table 2: Efficiency of the electron selection for simulated electrons and pions for energies between 10 and 50 GeV. Muons are simulated at 150 GeV. The efficiency is defined as the number of events after selection over the number of event before selection and it is estimated from Monte-Carlo.

Beam Energy	ε_μ	ε_e	ε_π
10 GeV	<0.1%	96%	15.9%
15 GeV	<0.1%	95.7%	10.1%
20 GeV	<0.1%	95.2%	6.3%
30 GeV	<0.1%	93.9%	2.3%
40 GeV	<0.1%	92.7%	1.2%
50 GeV	<0.1%	91.5%	1.1%

was developed. The method is the following: all the hits in an event are ordered in time; For each hit with a time over 50 ns, the number of hits in a timing window of 30 ns after the hit time is counted. If the number of hits is above 5, it is classified as a *late cluster*. The event is rejected if there is at least one late cluster. The multi-particle event rejection has been checked on simulated data and affects the selection between <0.1% up to 2% from 10 to 90 GeV pions. These multi-particle events are also suppressed in data. The number of events removed varies between 0.1% and 1% depending on the beam energy. However, due to the calorimeter not being fully equipped thus providing limited information, some contamination by multi-particle may remain in the data. The table 9 shows the selection cuts for the pion data. The selection efficiencies are shown in 3

Table 3: Efficiency of the pion selection for beam energies between 10 and 90 GeV. Muons are simulated at 150 GeV. The efficiency is defined as the number of events after selection over the number of event before selection and it is estimated from Monte-Carlo.

Beam Energy	ε_μ	ε_e	ε_π
10 GeV	<0.1%	<0.1%	29.9%
30 GeV	0.9%	<0.1%	50.3%
50 GeV	0.9%	<0.1%	51.1%
70 GeV	0.9%	<0.1%	51%
90 GeV	0.9%	<0.1%	50.2%

5. Timing calibration of the AHCAL

In a first step, the muon data is used to determine the parameters for the timing calibration. Muons are used because the process they induce is quasi-instantaneous. In a second step, the calibration is cross-checked using the electron data as also EM showers are quasi-instantaneous. This enables a verification of the time calibration procedure and may reveal effects that are not present in the muon data.

5.1 Time recording in the SPIROC2b

The SPIROC2b ASIC can readout 36 SiPM-channels. It is capable to measure the charge with two gains (high and low gain) and the time for each channel. Each channel is equipped with an analog memory, called memory-cells, with a depth of 16 events to store the energy and time measurement. Additionally, the ASIC can be operated in external or auto-trigger mode with a configurable threshold. The ASIC has two multiplexed TDC voltage ramps to avoid deadtime between each clock cycle. The two voltage ramps are common to all channels on the ASIC. The time information provided by the SPIROC2b in the data is in TDC units. Similar to the ADC scale, it would be difficult to compare directly channels using the TDC unit. The TDC information needs to be interpreted into a common unit of time, the nanosecond. The TDC information of each channel can be converted into nanoseconds following the schematic shown in figure 4.

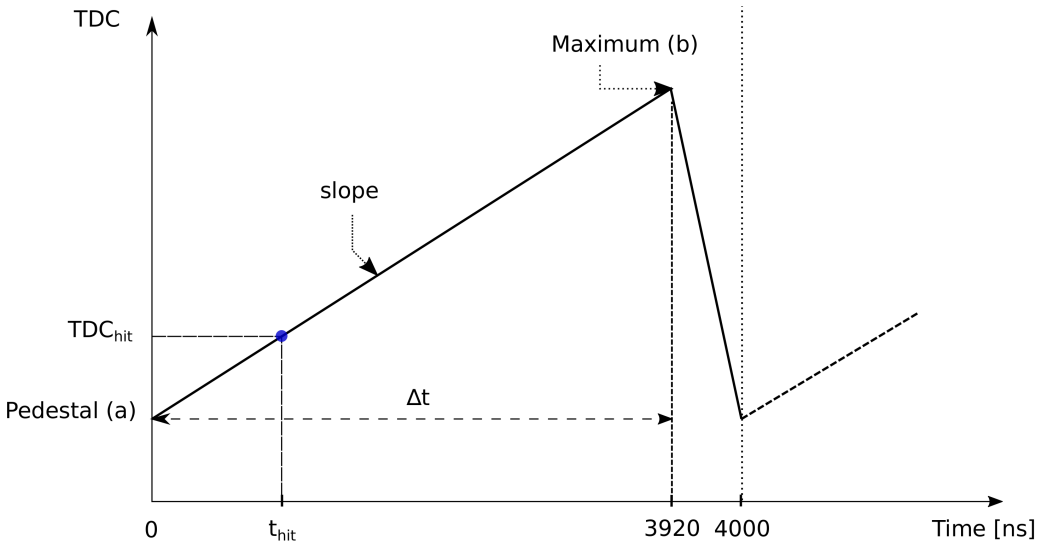

Figure 4: Schematic of the TDC ramp in the SPIROC2b used in testbeam with a slow clock of 250 kHz. The slope of the ramp is $s = (Max - Ped)/\Delta_t$.

In order to determine the ramp slope, the starting point or pedestal of the ramp and the endpoint of the ramp are measured. Since the SPIROC2b has two TDC ramps, each defined by the parity (even or odd) of the clock cycle counter or bunch-crossing ID (BXID), two slopes need to be extracted per chip. The differences between memory-cells lead to offsets in pedestals, thus 16 calibration values are needed per channel. The time of the hit in the i-th channel is then calculated as the following:

$$t_i[ns] = 1/s \times (TDC_i - Ped) \tag{5.1}$$

where Ped is the pedestal of the i-th channel in the first memory cell without taking into account the bunch-crossing parity. The extraction of the slope and the determination of the pedestal is described in the following sections.

5.2 Timing calibration procedure

The timing calibration procedure of the AHCAL is quite complex. An overview of the steps performed for the time calibration of each individual AHCAL channel is shown in figure 5.

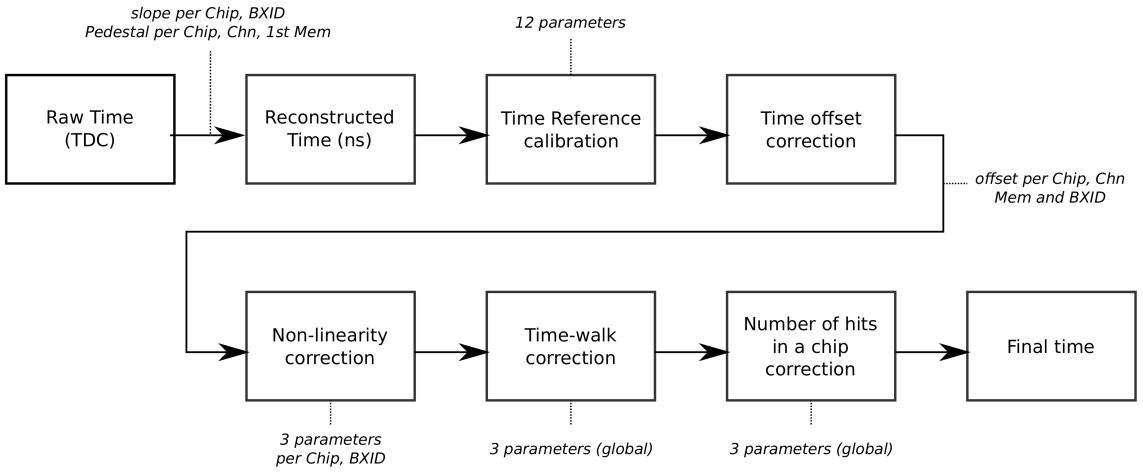

Figure 5: Overall view of the different steps performed for the AHCAL timing calibration. In total, more than 20000 constants are needed.

5.3 Slope and Pedestal extraction

To reconstruct the time in a channel, the TDC value measured needs to be converted into nanoseconds. The slope is calculated as

$$s\,[\text{TDC/ns}] = \frac{b-a}{3920} \tag{5.2}$$

where s is the TDC ramp slope, b is the endpoint of the TDC ramp and a is the start point of the TDC ramp that is referred to in the following as the pedestal. The total length of the ramp is 3920 ns instead of the expected value of 4000 ns due to a deadtime of around 2% [14] induced by the multiplexer that switches between the two TDC ramps.

To first order, the slope of the TDC ramp is assumed to be linear. The parameters a and b are extracted from the TDC spectrum per chip (combining all channels) and BXID parity using only the first memory-cell as shown in figure 6a. The TDC ramp slope does not depend on the memory-cell as the memory-cell only introduce an offset on the parameters a and b. A total of 208 slopes have to be extracted for the testbeam setup.

The extracted values for the inverse of the slope are shown in figure 6b. They are in the expected range of 1.6 ns per TDC bin due to the limited dynamic range provided by the chip, of around 2500 TDC bins for 4 μs.

The same method is used to determine the pedestal for each channel using only the first memory cell without taking into account the bunch-crossing parity. Any time offsets introduced by the other memory cells and the bunch-crossing parity are corrected in section 5.5.

5.4 Time reference calibration

The time references shown in table 6 are calibrated using the same method described above. However, to guarantee the most accurate result, the pedestal value is extracted for each memory cell. Since a signal with defined amplitude was injected in these channels, a corresponding amplitude range is required to reject noise hits from these channels. As these channels receive the trigger signal at the same time, a 2^{nd} order polynomial correction w.r.t T_{14} is done to remove any effects

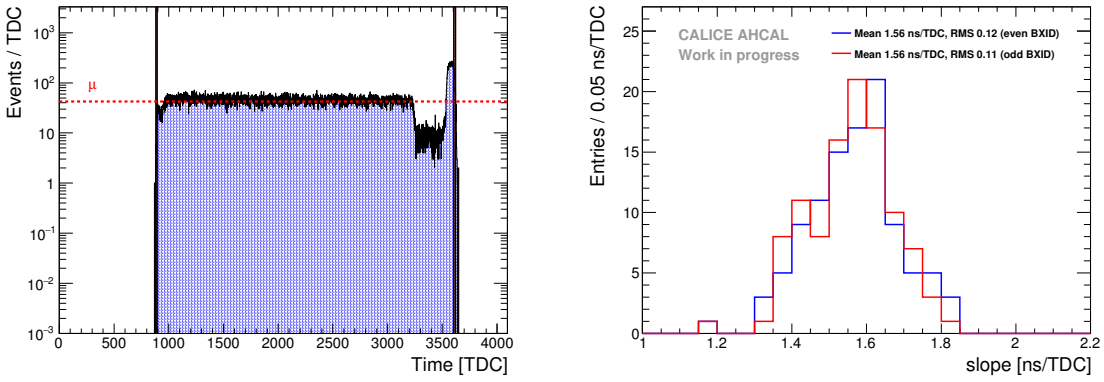

(a) (b)

Figure 6: a) TDC spectrum of a typical chip. The vertical black lines indicate the fitted Max and Pedestal parameters for this chip. The horizontal red line represents the mean μ of the histogram on the y-axis used for the determination of the parameter a. The extracted parameters are $1/s$ = 1.44 $\pm$ 0.01 ns/TDC, a = 888 $\pm$ 5 TDC and b = 3613 $\pm$ 8 TDC. b) Distribution of the fitted slopes for even and odd bunch-crossing IDs. μ_{odd} = 1.564 ns/TDC, RMS$_{odd}$ = 0.121, μ_{even} = 1.556 ns/TDC, RMS$_{even}$ = 0.113. In total, 208 TDC slopes were extracted.

induced by the front-end electronics. This correction is equivalent to a non-linearity correction of T_{12} and T_{13} relative to T_{14} similar to the procedure shown in section 5.6. In this case, T_{14} is not corrected for non-linearity.

Ideally, the T_{12} - T_{14} and T_{13} - T_{14} distributions should be a Gaussian distribution centered at 0 ns. The figure 7a shows the distribution of T_{12} - T_{14} before and after the correction. One can notice two peaks before the correction because of the fact that the pedestal value is dependent on the bunch-crossing parity.

Finally, the time reference is calculated as the mean of T_{12}, T_{13} and T_{14} per event. To reject events with a too large time reference uncertainty, a cut of 4 ns on the time reference uncertainty is applied. The mean uncertainty of the time reference is around 1.30 ns as shown in figure 7b. This resolution from the time reference contributes to the final timing resolution obtained.

5.5 Time offset correction

The time reference of the trigger is delayed compared to the muon passing through the detector because of the length of cables and the trigger electronics logic. Therefore, the time offset of the time reference is determined from data. The physical process induced by muons is instantaneous, therefore the difference of the hit time and the time reference for each channel, memory cell and BXID should be a distribution that is centered at 0 ns.

A shifting procedure of the time of the hit relative to the time reference for each channel, memory-cell and BXID parity is performed. This is done to take into account the delay time of the trigger due to cabling and the trigger electronics as well as possible differences in channel pedestals. Only memory-cells containing more than 100 events are considered. The histogram range of the time of the hit relative to the time reference is reduced iteratively, in the range $t_{max} \pm RMS$ with t_{max}

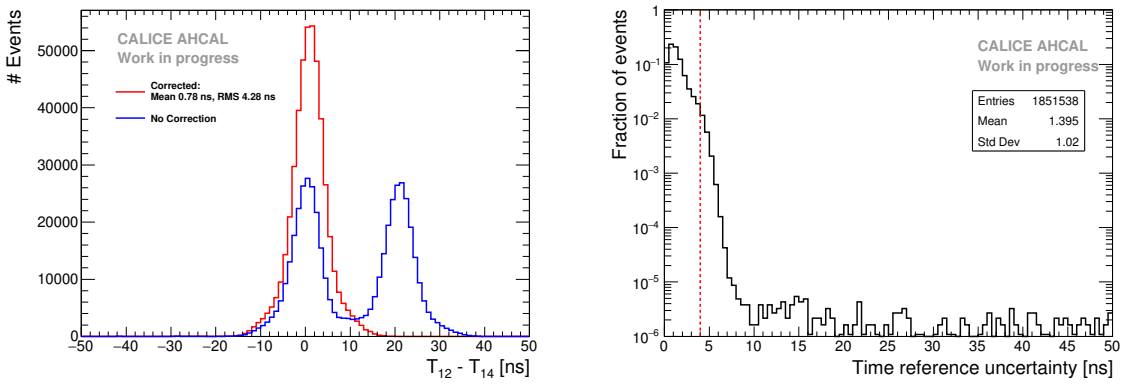

(a) (b)

Figure 7: a) Time difference between the trigger channels before and after correction for T_{12} and T_{14}. $\mu_{corrected}$ = 0.9 ns, $RMS_{corrected}$ = 4.8 ns. The two peaks in blue are due to the fact that the pedestal value is dependent on the bunch-crossing parity. b) Distribution of the time reference uncertainty. The red line represents the cut of 4 ns.

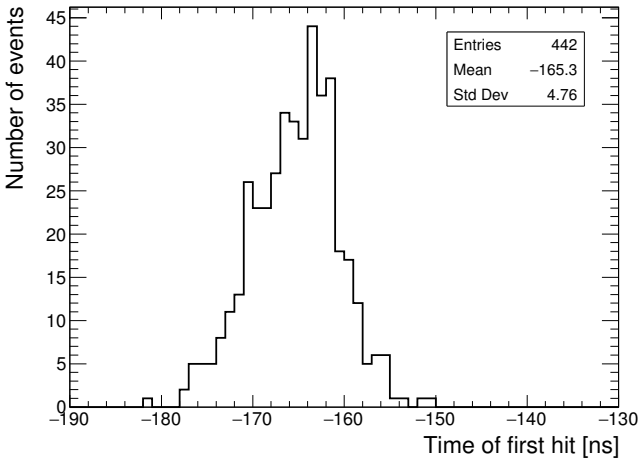

Figure 8: Time of first hit distribution for a single channel (Chip 236, Chn 21, Mem 01, BXID 1). An offset of -165.3 ns is determined for this channel.

corresponding to the time at the center of the maximum bin of the histogram, until the RMS of the distribution is smaller than 10 ns. This value was chosen because it corresponds to more than 3 sigma of the mean time reference uncertainty. The mean of the histogram is then used as the time offset value. An example of a single channel is shown in figure 8.

In total, 21040 individual offsets are extracted from data. The mean value of the time offset is around -150 ns which is around the expected value considering the cabling length and the trigger logic delay.

5.6 Non-linearity correction

The time calibration relies on the linearity of the TDC voltage ramp in the *SPIROC2B*. However,

this assumption is not entirely reliable as described in [15, 14]. The voltage slope shows a slight kink around the middle thus leading to a non-linear ramp. For this, a correction of the non-linearity is applied. By investigating the time of the first hit for each chip and BXID parity as a function of the TDC value of the hit, the shape of the graph indicates how reliable is the assumption of a linear ramp. If the ramp would be perfectly linear, one would obtain a flat graph. To correct for the non-linearity of the ramp, a 2^{nd} order polynomial is used. An example for a typical chip is shown in figure 9a. The non-linearity correction results in an improvement in the timing resolution (RMS) of the AHCAL by about 5.1% as shown in figure 9b.

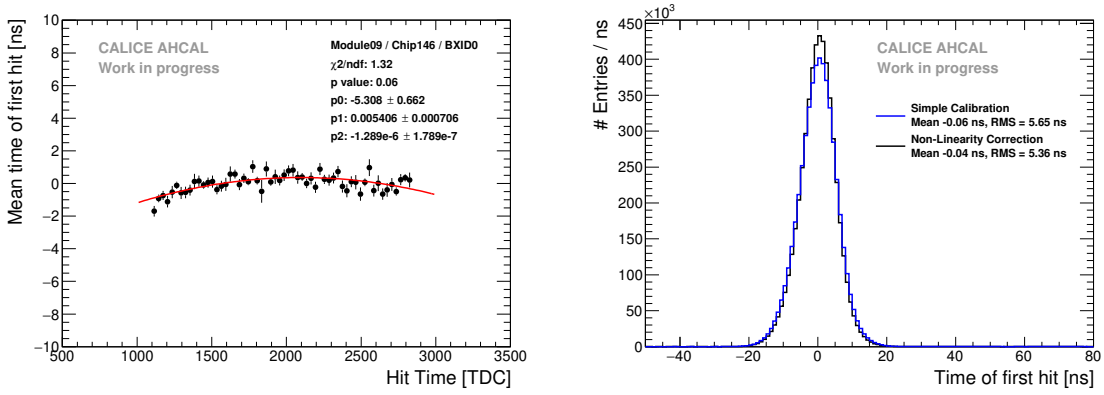

(a) (b)

Figure 9: a) Quadratic fit of chip 146 (BXID even) on layer 9. The graph is slightly curved showing that this chip presents a non-linear TDC ramp. b) Time of the first hit distribution before and after the non-linearity correction. The correction results in an improvement of around 5% on the RMS of the distribution.

5.7 Time-walk correction

The time-walk effect is due to the presence of an energy threshold that induces a time shift between a small amplitude signal and a high amplitude signal. Small amplitude signals will systematically trigger at a later time than high amplitude signals for a shaper that makes the signals peak at the same time. A time correction is determined by looking at the time of the first hit as a function of the amplitude of the hit as shown in figure 10a. This may be particularly relevant for late energy depositions in hadron showers that comes generally from neutrons depositing little energy in the calorimeter. An improvement of around 3% is achieved on the time resolution of the AHCAL as shown in figure 10b.

5.8 Number of triggered channel in a chip correction

After the time calibration, electrons show a significantly worse time resolution than muons. This was traced back to events where there are many channels that are triggered in the same chip. The mean time of first hit as a function of the number of triggered channels above 0.5 MIP in a chip, $N_{trig/chip}$, is shown in figure 11a. A time shift of up to 20-40 ns can be seen depending on $N_{trig/chip}$. The cause of the observed effect is most likely due to an element in the chip called a *delay box* that

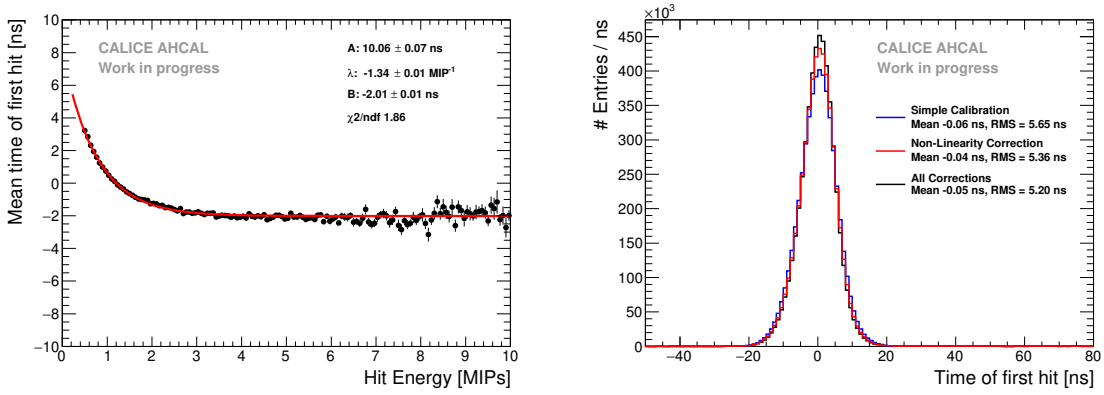

(a) (b)

Figure 10: a) Time of first hit as a function of the hit energy. A difference up to 6 ns is seen between small and large amplitudes. Time-walk correction extracted from data. The fit function is of the form $A \times e^{-\lambda x} + B$. b) Time of the first hit distribution before and after the time-walk correction. The correction results in an improvement of around 3% on the RMS of the distribution.

gets unstable with a high charge going through the chip. This chip element is responsible for the hold signal of the TDC ramp in the chip. The hold signal is delayed, and thus a higher TDC ramp value than the one expected is sampled.

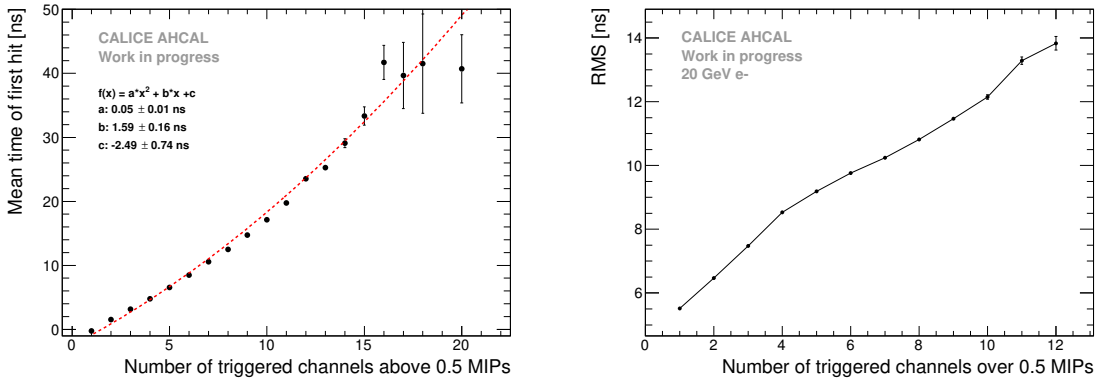

(a) (b)

Figure 11: a) Mean time of the first hit as a function of the number of triggered channels above 0.5 MIP, $N_{trig/chip}$, in a chip. The mean time shift upwards with the increase of triggers leading to large tails in the time distribution. A second order polynomial fit is done for the time correction shown by the red dashed line. b) RMS of the time distribution for 20 GeV electrons as a function of $N_{trig/chip}$.

Not only this effect shifts the mean time of the hit but as well it increase the RMS of the time distribution as shown in figure 11b for 20 GeV electrons. In order to determine a reliable time correction, the time correction parameters are determined combining all the electron data. This effect may be chip-dependent and the parameters for the correction may differ from chip to chip.

However, the limited amount of data does not allow to determine a correction function for each chip. In addition, the layers deeper in the calorimeter, which are most interesting for the pion analysis, are not reached by electrons. Therefore, a global function is used to correct the time in the data. This effect is parametrized in simulation as explained in section 3.1.

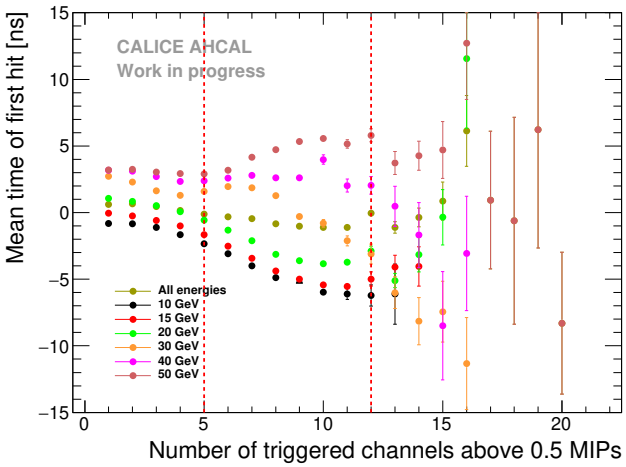

Figure 12: Residuals of the mean time of the first hit as a function of the number of triggered channels above 0.5 MIP in a chip after correction. The correction has been applied to all electron samples separately to evaluate the systematic uncertainty. The vertical red lines delimit the three sections used for the systematic uncertainty.

Figure 12 shows the residuals of the mean time of first hit as a function of $N_{trig/chip}$ after the correction. The correction has been applied to all electron samples separately in order to evaluate the systematic uncertainty of the correction. Three ranges in $N_{trig/chip}$ have been defined delimited by the red lines to estimate the uncertainty. To not overestimate the uncertainty, half of the residual envelope is taken as uncertainty. For $0 < N_{trig/chip} < 5$, a systematic uncertainty of 2 ns is taken, For $5 \leq N_{trig/chip} < 12$, a systematic uncertainty of 5 ns is taken and finally for $N_{trig/chip} \geq 12$, a systematic of 7 ns is taken. Finally, the uncertainty for the mean time of the hit is computed *for each bin of energy and radius* by weighting according to the fraction of hits in each of the three regions following equation 5.3. As the uncertainties in the three ranges are correlated, a conservative way is to add linearly the uncertainties.

$$\sigma = n_1 \times \sigma_1 + n_2 \times \sigma_2 + n_3 \times \sigma_3 \tag{5.3}$$

with σ_1 = 2 ns, σ_2 = 5 ns, σ_3 = 7 ns, n_1 the fraction of hits for the i-th bin in the region 0 $< N_{trig/chip} <$ 5, n_2 the fraction of hits for the i-th bin in the region $5 \leq N_{trig/chip} <$ 12 and n_2 the fraction of hits for the i-th bin in the region $N_{trig/chip} \geq 12$ and such as $n_1 + n_2 + n_3$ is equal to one in the i-th bin.

6. Results

6.1 Systematic uncertainties

Systematic uncertainties are evaluated in order to perform a significant assessment of differences observed between data and simulations. The following sources of systematic uncertainty are taken into account for data:

- Non-Linearity correction: A correction for the non-linearity of the TDC ramps is determined from data with a limited accuracy, leading to a systematic uncertainty. The residuals of the correction give a systematic uncertainty at the level of 0.2 ns.
- Time walk correction: Similarly to the non-linearity correction, the systematic uncertainty obtained from the residuals of the time walk correction in data is in the order of 0.2 ns.
- Number of triggered channels correction: The correction in data for $N_{trig/chip}$ results in a residual on the mean time of the first hit as shown in section 5.8. The uncertainty for the mean time of the hit in bins of energy and radius is calculated by weighting according to the fraction of hits in the regions of 0-5, 5-12 and over 12 in $N_{trig/chip}$ with an uncertainty of 2, 5 and 7 ns respectively. The resulting systematic uncertainty varies between 2 to 3.9 ns. For the time of first hit distribution, a systematic uncertainty is applied bin-by-bin for electrons and pions in the region of -30 ns to 30 ns. Outside of this region, a systematic error of 50% is taken. This systematic uncertainty is the most dominant over all other uncertainties.
- AHCAL energy scale: The energy scale of the AHCAL was determined using the muon dataset. A systematic uncertainty on the MIP scale of around 3.6% was derived by dividing the muon sample in odd and even run numbers and by looking at the average spread of the fitted MIP value for both subsamples. This is converted to an uncertainty in time using the mean time of first hit as a function of the hit energy using the QGSP_BERT_HP physics list. At 0.5 MIP, this results in an uncertainty of 0.1 ns. For hits above 1 MIP, the uncertainty is below 0.05 ns.

The following systematic uncertainties are taken into account for the simulation:

- Global time smearing parameters: A global time smearing parametrization is used from muon data to smear the time in simulation. A bin-by-bin systematic uncertainty is applied to the time of first hit distribution in simulation to take into account the difference with a layer-wise time smearing parametrization.
- Time smearing as function of $N_{trig/chip}$: A smearing parametrization of the width of the time distribution as a function of $N_{trig/chip}$ is obtained from electron data. An error band on the width was obtained by comparing all electron energies. The minimum and maximum borders of the error band are used to derive a systematic uncertainty for the simulation.
- Determination of the offset to $t = 0$: For simulation, the time shift per layer is calculated using a time of flight correction $T_{of} = \frac{z_{layer}}{c}$ with c the speed of light and z_{layer} the z position of a layer. For this, an uncertainty of 3 mm corresponding to the scintillator thickness is taken in z corresponding to 0.01 ns uncertainty in timing.

- Cross-talk: No measurement for optical cross-talk between tiles is available. From previous measurements with the AHCAL physics prototype, the cross-talk value varies between 10% and 18%. The cross-talk value induces a different number of hits in the detector thus has an impact on the width of the time of first hit distribution. The variation of this parameter in the simulation for the modules 4 to 10 is used for systematics.

- Normalisation of the pion dataset: When comparing the number of hits per time bin between data and simulation, there is an uncertainty related to the number of true pion events in the dataset. This number is perfectly known for simulation, however in data, an uncertainty is present due to some possible contamination from multi-particle events may be present still after the selection. The cluster time rejection method (see section 4.3) rejects up to 1% of events in the data. A conservative uncertainty of 10% on the data normalization is assigned when comparing data to simulation for the absolute time of first hit distribution of pions.

The systematic uncertainties are added in quadrature for the full systematic uncertainty assuming no correlation between uncertainties. For the mean time of the first hit as a function of the hit energy and as a function of the hit distance to the shower center of gravity, the systematic uncertainty is resulting at 0.3 ns for muons and between 2 to 4 ns for electrons and pions. The table 4 summarizes the systematic uncertainties used in the analysis.

Table 4: Summary of systematic uncertainties.

Uncertainty source	Full uncertainty
Non-linearity correction	0.2 ns
Time-walk correction	0.2 ns
Number of triggered channels correction	2 - 3.9 ns / bin-wise (e/π)
Energy Scale	0.05-0.1 ns
Time of flight offset	0.01 ns (MC)
Cross-talk parameter	10-18% (MC)
Global time smearing parameters	bin-wise (MC)
Number of triggered channels in a chip parametrization	bin-wise (MC)
Multi-particle events	10% (π)
Resulting systematic uncertainties per distribution	
data-MC ToFH distribution	bin-wise (e) - bin-wise + 10% (π)
data-MC vs hit energy	0.3 ns (μ) - 2 to 4 ns (e/π)
data-MC vs hit distance to shower CoG	0.3 ns (μ) - 2 to 4 ns (e/π)

6.2 Timing of muon and electron beams

The comparison of the time of first hit distribution for muons between data and simulations is shown in figure 13. The comparison shows that in the range of -20 ns to 20 ns, data and simulation agree well within the uncertainties. In this range the smearing with a double-Gaussian in the simulation describes the data well. However, outside this range, the simulation underestimates the tails. This

is probably caused by the noise implementation in simulation that does not perfectly reproduce the data. The time of the first hit distribution has been checked layer-by-layer and compared to simulations. Similarly, the agreement between data and simulations is best in the range of -20 ns to 20 ns and the tails are not perfectly reproduced in simulation.

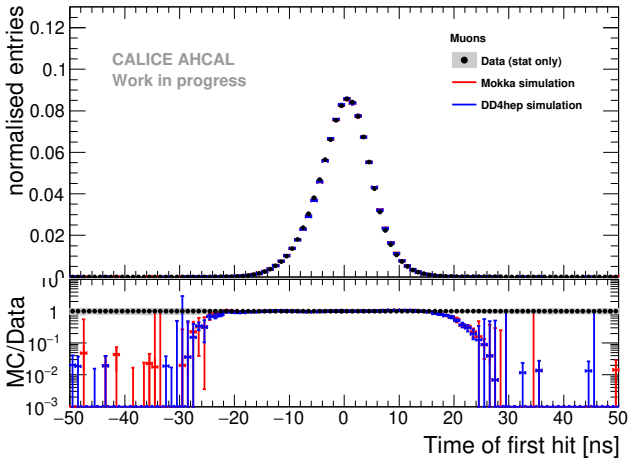

Figure 13: Time of first hit distribution for muons in data and both MOKKA and DD4HEP simulations between -50 and 50 ns. The grey area represents the statistical uncertainty of the data. The error bars of the simulation are obtained by varying the cross-talk parameter between 10% and 18% and taking into account the error of a global time smearing parametrization.

In order to further validate the time simulation, a comparison with electron data has been done. Figure 14a shows the comparison of the time of first hit distribution for 50 GeV electrons in data and simulation. The simulation is slightly wider than the data. This is caused by the simulation having more hits in a chip than data which can be seen in figure 14b. The simulation is higher than data in the region of 10 to 14 hits per chip. Overall, the simulation describes well the data within statistical and systematic uncertainties in the central region of -30 ns to 30 ns for all energies. The large error bars in the simulation are due to the parametrization of the increase of the width. However, the description of the tails of the time of first hit distribution in the simulation are well underestimated. Like for muons, this is due to the description of the noise in the simulation that is not perfectly reproduced.

6.3 Timing of pion showers

Figure 15 shows the distribution of the time of first hit compared to three different physics lists for 50 GeV pions. For the core of the distribution below 50 ns, all physics lists describe the data within the systematics. The late tail is described best by the QGSP_BERT_HP and QBBC physics lists. The QGSP_BERT physics list without the precision treatment of neutron results in an overestimation of the tail of the distribution by around a factor of 5.

The dependence of the time of first hit on the hit energy is studied in the following. It is expected that there is no hit energy dependence for muon and electron beams as these are quasi-instantaneous. On the other hand, for pions, it is expected that low energy hits mostly coming from

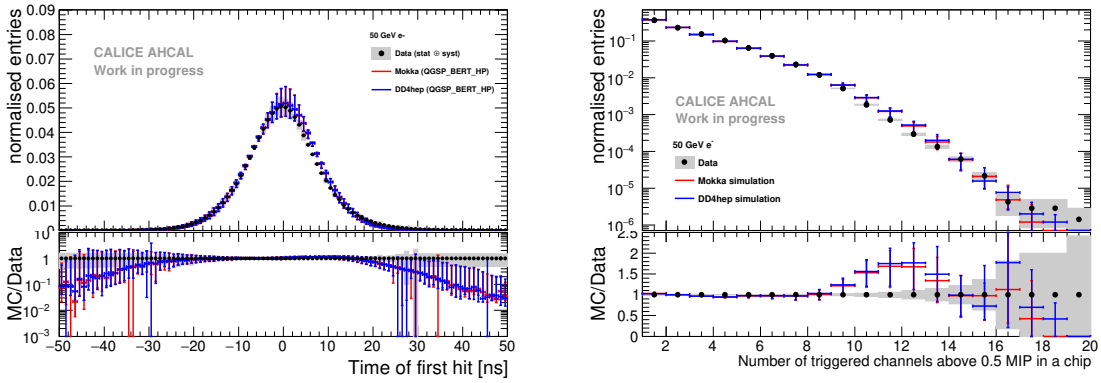

(a) (b)

Figure 14: a) Comparison of the time of first hit between data and both MOKKA and DD4HEP simulations for 50 GeV electrons. The grey area represents the statistical and systematical error of the data. Error bars in simulation are obtained by varying the cross-talk parameter between 10% and 18% and with the uncertainty on parametrization of the width of the time distribution as a function of the number of triggered channels in a chip. b) Comparison of the number of triggered channels per chip between data and simulations for 50 GeV electrons. The grey area represents the statistical error of the data. Error bars in simulation are obtained by varying the cross-talk parameter between 10% and 18%.

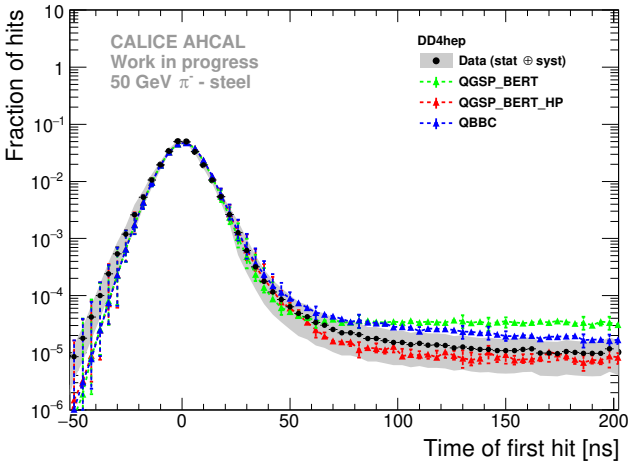

Figure 15: Comparison of the time of first hit distribution for 50 GeV pions in data and three different physics list for the DD4HEP simulation. The grey and color bands shows the statistical and systematic uncertainties.

neutron signals in the calorimeter are delayed. Figure 16 shows the comparison of the mean time of first hit as a function of the hit energy in data and simulation for 50 GeV pions.

In general, data and all simulations show a rise of the mean time of first hit towards small hit energies, although the large systematic uncertainties on the data make a firm statement difficult.

This behaviour is consistent with the expectation that low energy hits are responsible for delayed energy depositions in the calorimeter, most likely due to low energy neutrons from capture and spallation processes, while higher energy deposits occur mostly in the prompt part of the hadron shower. The rise in data is located at hit energies below 1 MIP, while it extends up to 4 MIP in the simulation. A difference is visible between the physics lists mainly between hit energies of 1-3 MIPs, where QGSP_BERT_HP lies below QGSP_BERT and QBBC. In this range, and at higher MIP values, all physics lists agree within the large systematic uncertainties with the data.

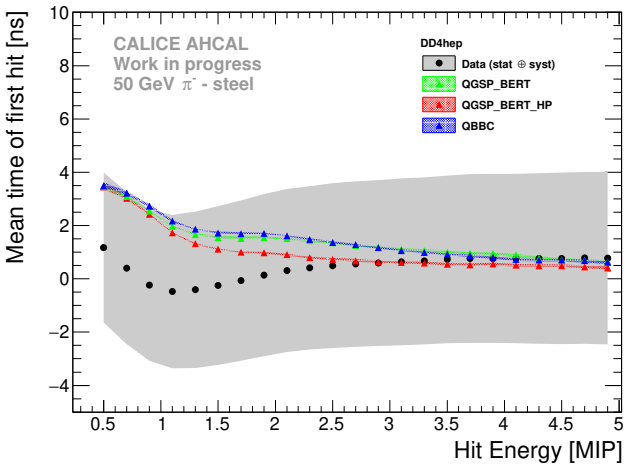

Figure 16: Comparison of the mean time of first hit as a function of the hit energy in data and DD4HEP simulation for 50 GeV pions. The grey and color bands shows the statistical and systematic uncertainties.

The prompt component of a hadron shower is dominated by EM sub-showers and relativistic particles, whereas the delayed component is coming from mostly evaporation and spallation low energy neutrons. It is expected that the former is concentrated near the shower axis, while the latter is spread out laterally as these neutrons can travel far away in the calorimeter before interacting. Therefore, the radial dependence of the time of first hit of 50 GeV pion showers is studied. It is studied separately for modules 3 to 10 (small modules) and modules 11 to 14 (big modules) as significant differences were found (figure 17). Both distributions show an increase of the mean time of first hit with the distance to the shower center, but the effect is larger for the small modules, where the mean time of first hit is around 9 ns at 22 cm, while the large modules show an effect of less than 4 ns at the same distance. For the modules 3 to 10, the QBBC and QGSP_BERT_HP physics lists reproduce well the data within systematics while QGSP_BERT lies above the data at large distances from the center-of-gravity of the shower. For the modules 11 to 14, the QGSP_BERT_HP physics list agrees the best with the data. The QBBC and QGSP_BERT physics lists agree with data up to around 10 cm distance and then both tend to lie above the data for higher distances. The observations for other beam energies are similar. The main difference between the QGSP_BERT_HP and the QGSP_BERT physics list is the detailed neutron tracking in QGSP_BERT_HP. The figures show that without this detailed neutron tracking, too many late energy depositions are created that are spread far away from the shower axis.

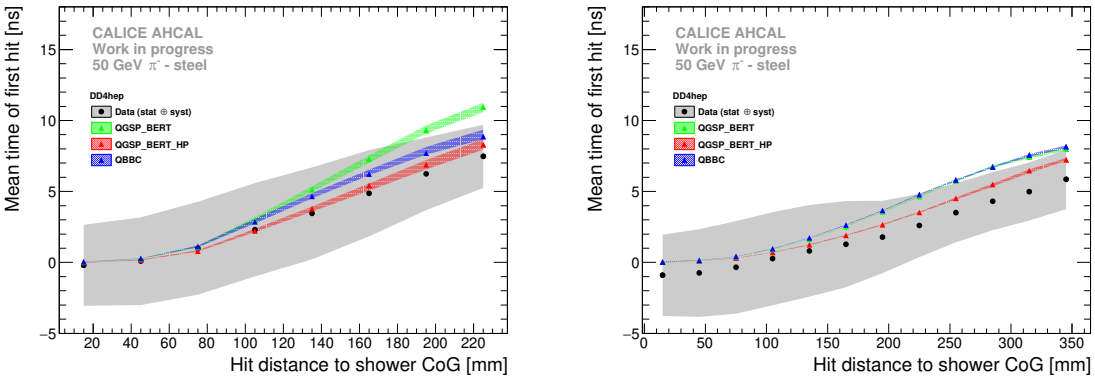

(a) Layers 3 to 10

(b) Layers 11 to 14

Figure 17: Comparison of the time of first hit as a function of the hit distance to the shower axis in data and simulations for 50 GeV pion for the modules 3 to 10 on the left and for modules 11 to 14 on the right. The grey and color bands shows the systematics.

By studying the modules individually, it was found that the mean time of the first hit as a function of the hit distance to the shower axis decreases with deeper modules as shown in figure 18a. Especially at larger distances this study shows strong statistical fluctuations. The simulation shows a similar behaviour (figure 18b). This behavior is related to where the pion shower starts and thus, at the depth that the shower is sampled. This has been verified by looking at the mean time of the first hit as a function of the hit distance to the shower axis at a fixed depth of the reconstructed shower start as shown in figure 19 and for different reconstructed shower start at a fixed layer as shown in figure 20 in the appendix.

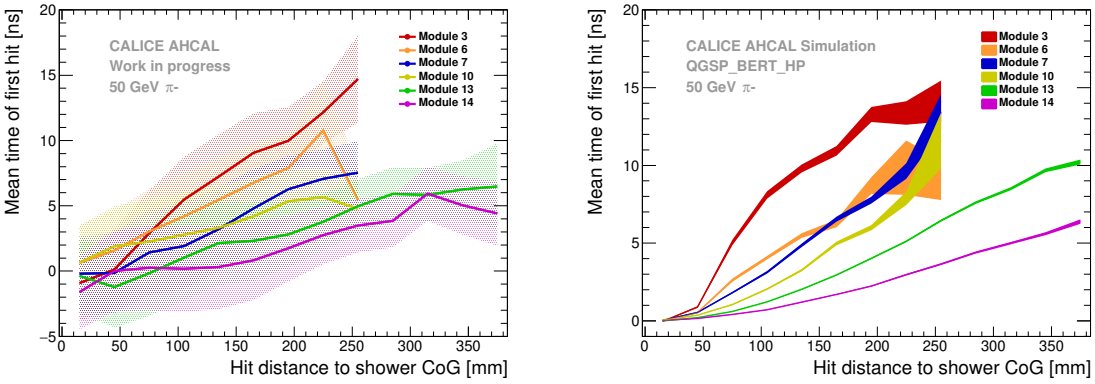

(a)

(b)

Figure 18: Mean time of first hit as a function of the hit distance to the shower axis for 50 GeV pions for different modules. For data, on the left. For simulation using the QGSP_BERT_HP physics list, on the right. Both figures shows the same behavior with a decrease of the curve slope for deeper modules in the calorimeter.

7. Conclusion

In this note, the timing study of the CALICE AHCAL prototype was presented, using the data taken with steel absorber at the CERN SPS in July 2015 in muon, electron and pion beams between 10 and 90 GeV. This prototype was partially instrumented with several generations of active readout boards which do not reach the final design performance. It was operated at a lower clock speed in order to have a good efficiency in the data taking. Nevertheless, the data collected has been used to develop calibration and correction procedures, to study systematic effects and understand the simulations that reproduce the data and allow for meaningful comparisons with hadron showers.

Firstly, the timing calibration was presented. A time resolution of around 5 ns was achieved with muons and around 8 ns with electrons. The increase of the time resolution for electrons is due to an electronic effect that increases the time resolution depending on the number of hits within a chip.

Secondly, the study of the time development of pion showers was presented. Late contributions are typically at low hit energies below 1 MIP and as well the late contributions are predominant at larger radius from the core of the shower. Comparisons to simulations show that the time structure of pion showers is well reproduced by the GEANT 4 physics lists QGSP_BERT_HP and QBBC. The QGSP_BERT physics list tend to over-estimate the late contribution, showing that a proper treatment of neutrons is needed to reproduce the data to a satisfactory level.

References

[1] M. A. Thomson, *Particle Flow Calorimetry and the PandoraPFA Algorithm*, *Nucl. Instrum. Meth.* **A611** (2009) 25–40, [arXiv:0907.3577].

[2] T. Barklow, L. d'Hautuille, C. Milke, B. Schumm, A. Schütz, M. Stanitzki, and J. Strube, *A Study of the Impact of High Cross Section ILC Processes on the SiD Detector Design*, arXiv:1609.0781.

[3] A. Benaglia, E. Auffray, P. Lecoq, H. Wenzel, and A. Para, *Space-time development of electromagnetic and hadronic showers and perspectives for novel calorimetric techniques*, *IEEE Transactions on Nuclear Science* **63** (April, 2016) 574–579.

[4] F. Sefkow and K. Krueger, *Towards a new AHCAL prototype*, CALICE Collaboration Meeting, Arlington (Texas, USA), 14 Sep 2016 - 16 Sep 2016, Sep, 2016.

[5] K. Krüger and the CALICE collaboration, *Prototype tests for a highly granular scintillator-based hadron calorimeter*, *Journal of Physics: Conference Series* **587** (2015), no. 1 012033.

[6] S. Callier, F. Dulucq, R. Fabbri, C. de La Taille, B. Lutz, G. Martin-Chassard, L. Raux, and W. Shen, *Silicon photomultiplier integrated readout chip (spiroc) for the ilc: Measurements and possible further development*, in *2009 IEEE Nuclear Science Symposium Conference Record (NSS/MIC)*, pp. 42–46, Oct, 2009.

[7] J. Kvasnicka, *A scalable data acquisition system for the calice tile hadron calorimeter*, in *2016 IEEE Nuclear Science Symposium, Medical Imaging Conference and Room-Temperature Semiconductor Detector Workshop (NSS/MIC/RTSD)*, pp. 1–6, Oct, 2016.

[8] P. Mora de Freitas and H. Videau, *Detector simulation with MOKKA / GEANT4: Present and future*, in *Linear colliders. Proceedings, International Workshop on physics and experiments with future electron-positron linear colliders, LCWS 2002, Seogwipo, Jeju Island, Korea, August 26-30, 2002*, pp. 623–627, 2002.

[9] M. Frank, F. Gaede, C. Grefe, and P. Mato, *DD4hep: A Detector Description Toolkit for High Energy Physics Experiments*, *J. Phys. Conf. Ser.* **513** (2014) 022010.

[10] S. Agostinelli and al., *Geant4 – a simulation toolkit*, *Nuclear Instruments and Methods in Physics Research Section A: Accelerators, Spectrometers, Detectors and Associated Equipment* **506** (2003), no. 3 250 – 303.

[11] The CALICE collaboration, *Construction and commissioning of the CALICE analog hadron calorimeter prototype*, *Journal of Instrumentation* **5** (2010), no. 05 P05004.

[12] O. Hartbrich, *Scintillator Calorimeters for a Future Linear Collider Experiment*. PhD thesis, Hasylab, DESY, Hamburg, 2016.

[13] C. Günter, *Comparison of Iron and Tungsten Absorber Structures for an Analog Hadron Calorimeter*. PhD thesis, U. Hamburg, Dept. Phys., Hamburg, 2015.

[14] E. Brianne, "Studies of the front-end electronics of the Analog HCAL." DESY summer student report, 2012.

[15] O. Hartbrich, "Investigation of the time measurement capabilities of the SPIROC2b ASIC." DESY summer student report, 2011.

A. Appendix

Table 5: List of runs taken at SPS in July 2015.

Particle	**Energy**	**Runs**	**# Events**
μ^-	50 GeV	24016-24204	120,887,651
	150 GeV	24623-24662	15,534,328
e^-	10 GeV	24531-24576	38,028,438
	15 GeV	24507-24527	7,701,325
	20 GeV	24479-24504	10,498,554
	30 GeV	24454-24475	3,382,943
	40 GeV	24420-24448	2,665,843
	50 GeV	24404-24419	5,933,995
π^-	10 GeV	24266-24272, 24300-24317, 24381-24397	24,311,420
	20 GeV	24398-24400	N/A*
	30 GeV	24259-24299, 24319-24380	10,120,753
	50 GeV	24212-24254, 24325-24357, 24580-24612	10,704,661
	70 GeV	24219-24242, 24365-24374	8,885,407
	90 GeV	24233-24287, 24331-24364	7,955,604

Table 6: List of AHCAL channels used as time reference for this analysis. In this analysis, the time reference signals T_{12}, T_{13} and T_{14} are used.

Layer #	Chip Number	Channel	Comments	Name
11	169	29	noisy	T_{11}
11	177	23	broken	-
12	185	29	-	T_{12}
13	201	29	-	T_{13}
13	211	6	broken	-
14	217	23	-	T_{14}

*Not analyzed due to limited dataset.

Table 7: Selection cuts for the muon runs.

Name	**Beam Energy**	**Cut**
Preselection	All	0 mm < cog_z < 800 mm
	All	0 < n_{hits} < 20
Track Selection (Modules 1 to 10)	All	n_{hits} in tower > 7
	All	n_{hits} in layer < 3
Track Selection (Modules 11 to 14)	All	n_{hits} in tower > 2
	All	n_{hits} in layer < 3

Table 8: Selection cuts for each electron runs.

Name	**Beam Energy**	**Cut**
Event Quality	All	Cherenkov ON
	All	Energy in the first 3 layers of AHCAL > 10 MIP
Electron Selection	10 GeV	25 < n_{hits} < 75
	15 GeV	30 < n_{hits} < 90
	20 GeV	40 < n_{hits} < 100
	30 GeV	50 < n_{hits} < 110
	40 GeV	60 < n_{hits} < 120
	50 GeV	70 < n_{hits} < 140
	All	cog_z < 250 mm
	All	-90 mm < $cog_{x,y}$ < 90 mm
	All	Energy in last two layers < 1% E_{sum}

Table 9: Selection cuts for the pions runs.

Name	**Beam Energy**	**Cut**
Event Quality	All	Cherenkov OFF
Pion Selection	All	n_{hits} > 20
	All	n_{hits} in the first 2 AHCAL layers < 5
	All	Energy in last two layers > 1% E_{sum}
Multi Particle Rejection	All	n_{hits} in time window > 5
	All	$n_{Cluster}$ > 0

Table 10: List of the different SiPMs used in the CALICE AHCAL in July 2015.

Layer	Producer	Model	Area (mm^2)	Pitch (μm)	WLS Fibre	Read-out type	N_{px} [10^3]
1	Hamamatsu	S12571_010P	1×1	10	no	Bottom	10
2	Hamamatsu	S10362-11-025O	1×1	25	no	Side	1.6
3	Hamamatsu	S12571-025P	1×1	25	no	SMD	1.6
4-5	Ketek	N/A	2.25×2.25	18	no	Side	12
6-10	CPTA	CPTA	1.28×1.28	40	yes	Side	0.8
11-12	Ketek (UHH)	PM1125NS-SB0	1.2×1.2	25	no	Side	2.3
13-14	SenSL	MicroFB-10020-SMT	1×1	20	no	Side	1.3

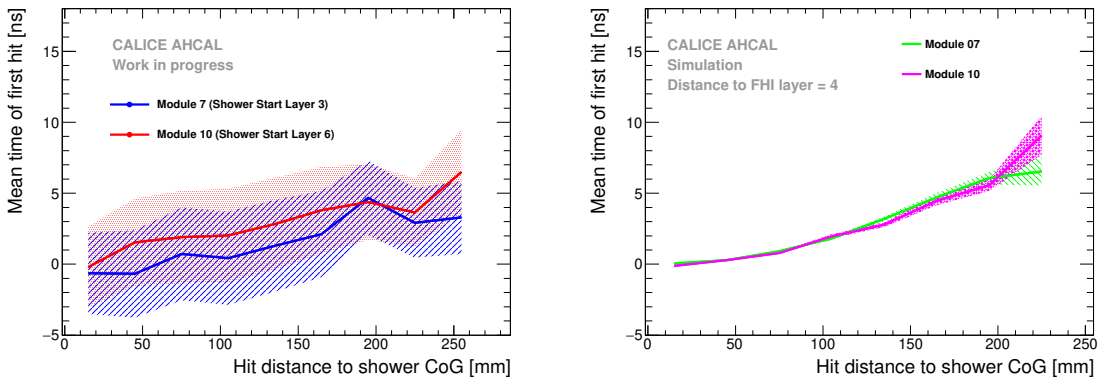

(a) (b)

Figure 19: Mean time of first hit as a function of the hit distance to the shower axis for 50 GeV pions for a fixed distance of 4 between the reconstructed FHI layer and a layer. The left plot shows the radial timing profile of modules 7 and 10 in data. The right plots shows the radial timing profile for the same layers in simulation with the QGSP_BERT_HP physics list.

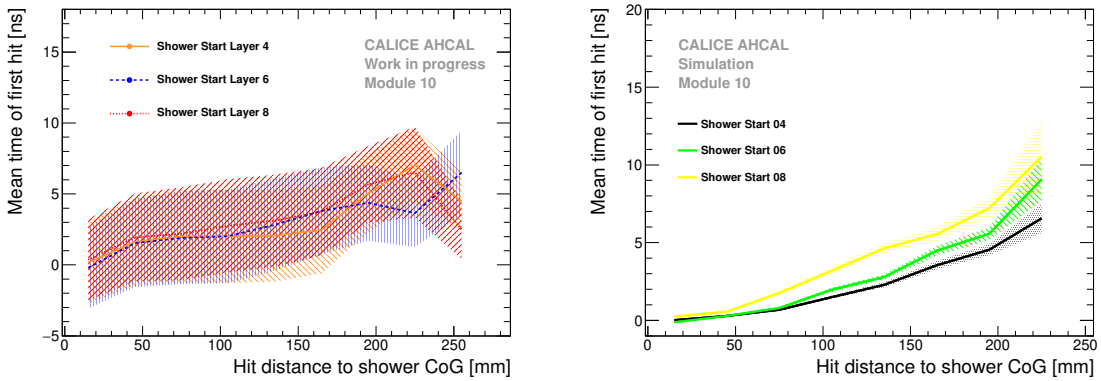

(a) (b)

Figure 20: Mean time of the first hit as a function of the hit distance to the shower axis for 50 GeV pions for different reconstructed FHI layers. In data on the left and in simulation with the QGSP_BERT_HP physics list on the right.